

## Lower-thermospheric wind fluctuations measured with an FPI during pulsating aurora at Tromsø, Norway

S. Oyama<sup>1,2</sup>, K. Shiokawa<sup>1</sup>, J. Kurihara<sup>1,\*</sup>, T. T. Tsuda<sup>1</sup>, S. Nozawa<sup>1</sup>, Y. Ogawa<sup>3</sup>, Y. Otsuka<sup>1</sup>, and B. J. Watkins<sup>2</sup>

<sup>1</sup>Solar-Terrestrial Environment Laboratory, Nagoya University, Nagoya, Japan

<sup>2</sup>Geophysical Institute, University of Alaska Fairbanks, Fairbanks, AK, USA

<sup>3</sup>National Institute of Polar Research, Tokyo, Japan

\* now at: Graduate School of Science, Hokkaido University, Sapporo, Japan

Received: 4 February 2010 – Revised: 22 September 2010 – Accepted: 27 September 2010 – Published: 6 October 2010

**Abstract.** Simultaneous observations were conducted with a Fabry-Perot Interferometer (FPI) at a wavelength of 557.7 nm, an all-sky camera at a wavelength of 557.7 nm, and the European Incoherent Scatter (EISCAT) UHF radar during the Dynamics and Energetics of the Lower Thermosphere in Aurora 2 (DELTA-2) campaign in January 2009. This paper concentrated on two events during periods of pulsating aurora. The lower-thermospheric wind velocity measured with the FPI showed obvious fluctuations in both vertical and horizontal components. Of particular interest is that the location of the fluctuations was found in a darker area that appeared within the pulsating aurora. During the same time period, the EISCAT radar observed sporadic enhancements in the F-region backscatter echo power, which suggests the presence of low-energy electron (1 keV or lower) precipitation coinciding with increase in amplitude of the electromagnetic wave (at the order of 10 Hz or higher). While we have not yet identified the dominant mechanism causing the fluctuations in FPI-derived wind velocity during the pulsating aurora, the frictional heating energy dissipated by the electric-field perturbations may be responsible for the increase in ionospheric thermal energy thus modifying the local wind dynamics in the lower thermosphere.

**Keywords.** Ionosphere (Auroral ionosphere; Ionosphere-magnetosphere interactions) – Meteorology and atmospheric dynamics (Thermospheric dynamics)

### 1 Introduction

Pulsating aurora is a typical phenomenon of the recovery phase of magnetic substorm and is frequently observed in the morning sector (Omholt, 1971). The pulsation period statistically lies in two ranges, 2–20 s and 0.2–0.5 s (Sandahl et al., 1980; Stenbaek-Nielsen, 1980; Yamamoto and Oguti, 1982; Yamamoto, 1988; Nemzek et al., 1995). While our understanding of pulsating aurora has not yet reached maturity, the widely accepted generation mechanism causing pulsations in precipitating electrons is related to wave-particle interactions around the equatorial plane in the magnetospheric tail (Sandahl et al., 1980; Yamamoto and Oguti, 1982; Yamamoto, 1988; Davidson, 1990). The closure current system in pulsating aurora may not be as strongly evolved as compared to that in the discrete arc because of smaller precipitation flux (or upward field-aligned current) and weaker perpendicular electric field (or the Pedersen current). Thus one may assume that Joule energy dissipation does not play an important role for modifications of the thermospheric wind dynamics during pulsating aurora.

Lower-thermospheric wind dynamics at auroral latitudes have been studied extensively using instruments such as Fabry-Perot interferometer (FPI), incoherent scatter (IS) radar, and satellites. One of the important issues remaining in this field is to gain a quantitative understanding of the ionospheric/thermospheric energy budget during periods of geomagnetic disturbance. Fluctuation in the lower-thermospheric wind velocity near discrete auroral arcs is an appropriate research objective because of coinciding enhancements in the electron density, the perpendicular electric field, the Joule/particle heating rate, and ion drag (Ishii et al., 2004, and references therein). In this paper we address the



Correspondence to: S. Oyama  
(soyama@stelab.nagoya-u.ac.jp)

lower-thermospheric wind variations during pulsating aurora as this has not yet been studied. Recent work by Hosokawa et al. (2008, 2009) showed the presence of electric-field fluctuations (about 5–10 mV m<sup>-1</sup>) in association with pulsating aurora. Theoretical predictions suggest that rapidly fluctuating electric fields can induce large enhancements in the Joule heating rate due to the time derivative term in the ion-momentum equation (Codrescu et al., 1995, 2000; Brekke and Kamide, 1996; Brekke, 1997; Matsuo et al., 2002, 2003, 2005; Shepherd et al., 2003; Matsuo and Richmond, 2008), although these studies did not specifically address the presence of electric-field perturbations in pulsating aurora.

The vertical component of the lower-thermospheric wind velocity is on average considerably smaller than the horizontal component (Oyama et al., 2005). However, it is well known that the vertical wind speed at high latitudes can fluctuate with notable amplitudes in excess of a few tens ms<sup>-1</sup> during periods of geomagnetic disturbance (Oyama et al., 2008, and references therein). Fluctuation in the vertical wind speed during disturbed periods can be regarded as a tracer to identify the thermospheric response to the geomagnetic activity because of quick response (within a few minutes) to changes in the geomagnetic activity (Kurihara et al., 2009; Kosch et al., 2010) and the nearly zero average of the vertical wind speed.

This paper focuses on two events for which wind fluctuations were measured with an FPI ( $\lambda = 557.7$  nm) at the Tromsø European Incoherent Scatter (EISCAT) radar site (geographic coordinate: 69.6° N and 19.2° E; geomagnetic coordinate: 66.7° N and 102.2° E; 6.4 L value) during pulsating aurora. The details of the experiment configuration are presented in Sect. 2. Section 3 shows the observational results. These observations of lower-thermospheric wind fluctuations within pulsating aurora are, to the best of our knowledge, the first report of such an occurrence, even though an in-situ measurement of the neutral wind velocity during pulsating aurora has been previously carried out using the trimethyl aluminum (TMA) trail released during the JOULE-II sounding rocket campaign (Sangalli et al., 2009). While we have not yet identified the dominant mechanism, if any, this paper discusses effects of the electric-field perturbation associated with pulsating aurora in Sect. 4. The summary and conclusions are presented in Sect. 5.

## 2 Experiment

Installation of the Fabry-Perot Interferometer (FPI) was made at the Tromsø EISCAT radar site in January 2009 to coordinate with the Dynamics and Energetics of the Lower Thermosphere in Aurora 2 (DELTA-2) campaign, the EISCAT UHF radar, and other ground-based optical and radio instruments. A Japanese S-310-39 rocket was launched from the Andøya Rocket Range at 00:15 UT on 26 January 2009. The FPI includes a filter wheel and a sky scanner allowing se-

quential measurements by selecting one of the optical filters (channel 1: 557.7 nm, channel 2: 630.0 nm, and channel 3: 732.0 nm) and directions of the line-of-sight (any azimuth and elevation angles). The diameter of the etalon is 116 mm. One of the notable characteristics is the number of fringes imaged on the CCD camera (1024 × 1024 pixels). More than ten fringes can be captured simultaneously in one CCD image due to relatively wide field-of-view (the full width of half maximum is about 4°). The Doppler shift or the line-of-sight speed is calculated from individual fringes then averaged for each image. The statistical standard deviation derived from the averaging process is taken as the measurement uncertainty and displayed as error bars in the plots presented in this paper. Data taken on 26 and 19 January 2009 are analyzed in this paper. The FPI was operated with the 557.7 nm optical filter. Four cardinal points with zenith angle of 15° and the geographic vertical (i.e. five directions) were measured sequentially. The exposure time at each position was 15 s and each sequence including the laser fringe measurement was 2 min 45 s. The combination of data from the four cardinal positions provides the horizontal components of the neutral wind velocity (see the methodology developed by Shiokawa et al., 2003).

A new all-sky camera (ASC, camera #12 of the Optical Mesosphere Thermosphere Imagers (OMTIs); Shiokawa et al., 2009) was also installed at the Tromsø EISCAT radar site. This camera includes a filter wheel used to select one of the six optical filters (channel 1: 557.7 nm, channel 2: 630.0 nm, channel 3: OH band (720 ~ 1000 nm), channel 4: 589.3 nm, channel 5: 572.5 nm, and channel 6: 732.0 nm). For the nights of 26 and 19 January 2009, the ASC was operated by choosing sequentially one of the optical filters among 557.7 nm (5 s), 630.0 nm (10 s), OH band (1 s), background (25 s), and 732.0 nm (30 s) (number in the parenthesis is the exposure time). The operating sequence represented by the channel number is 1, 2, 6, 1, 2, 6, 3, 1, 2, 6, 1, 2, 6, 3, 1, 2, 6, 1, 2, 6, 3, and 5. Data taken with the 557.7 nm filter are presented in this paper because it is the optimum wavelength to investigate the morphology of aurora, although the time resolution is not sufficient to estimate the pulsation frequency.

The pulsation frequency is estimated from data taken with a high-speed (29.97 Hz sampling rate) all-sky TV camera (with no optical filter) at the Tromsø site. First, areas for which the pulsating patches have relatively stable spatial features are selected visually, then the pulsation “on” and “off” intervals in the time domain are measured, and spectrum analysis with the Fast Fourier Transform method is performed. This process is better than analyzing data taken at a fixed point because we can avoid decreases in the pulsation period due to streaming patches across the fixed point (Yamamoto, 1988).

The EISCAT UHF radar was operated with two kinds of antenna position sequence as summarized in Table 1. The time interval between two successive antenna positions was about 90 s, and the duration of one antenna position sequence

**Table 1.** Antenna positions of the EISCAT UHF radar for the experiments on 26 and 19 January 2009. Azimuth angle is clockwise from north (e.g., 90° is east).

|                 | direction     | symbols  | azimuth | elevation |
|-----------------|---------------|----------|---------|-----------|
| 19 January 2009 | southeast     | SE       | 133.3°  | 56.8°     |
|                 | south         | S        | 166.5°  | 59.4°     |
|                 | field-aligned | $B_{//}$ | 185.8°  | 77.4°     |
|                 | vertical      | Z        | N/A     | 90.0°     |
| 26 January 2009 | southwest     | SW       | 226.7°  | 61.6°     |
|                 | south         | S        | 193.5°  | 64.0°     |
|                 | field-aligned | $B_{//}$ | 185.8°  | 77.4°     |
|                 | vertical      | Z        | N/A     | 90.0°     |

was 6 min. The pulse scheme used was “beata,” which is the 64 subcycle alternating codes employed by the EISCAT radars with 32 bits and 20  $\mu$ s baud length or about 3 km range resolution. The backscatter echo power every data dump (5 s) is presented in this paper.

### 3 Observational results

#### 3.1 Event 1: 26 January 2009

The EISCAT UHF radar operated from 17:00 on 25 January to 05:00 UT on 26 January. To understand the aurora activity that night, a meridional keogram was made from the all-sky camera (ASC;  $\lambda = 557.7$  nm) as shown in Fig. 1a. While there was no auroral activity for the first 4.5 h (17:00 to 21:30 UT), some auroral displays started at latitudes higher than 70° after 21:30 UT then moving equatorward down to 68° latitude at 00:00 UT. The substorm breakup occurred at 00:23 UT on 26 January. This temporal evolution of the auroral morphology is consistent with that in the x-component (meridional component) of the magnetometer data, which show obvious negative deviations or westward ionospheric current seen from Sørøya (SOR) to Pello (PEL) as presented in Fig. 1b.

While one cannot find signatures of pulsating aurora in the keogram due to low time resolution, pulsating aurora began equatorward of Tromsø 7 min after the breakup (i.e. at 00:30 UT) according to the high-speed all-sky TV camera. For the first 14 min after starting of the pulsation (i.e. from 00:30 to 00:44 UT), some bright discrete arcs randomly appeared in the northern half of the all-sky image from Tromsø while pulsating aurora remained in the southern half. After the last discrete arc moved past the westward horizon at 00:44 UT, the pulsating aurora came over the zenith of the Tromsø camera. The pulsating aurora that appeared from 01:15 to 01:40 UT was characterized by highly complex spatio-temporal behavior. Individual luminous patches surrounded by darker areas had irregular shapes; but tended

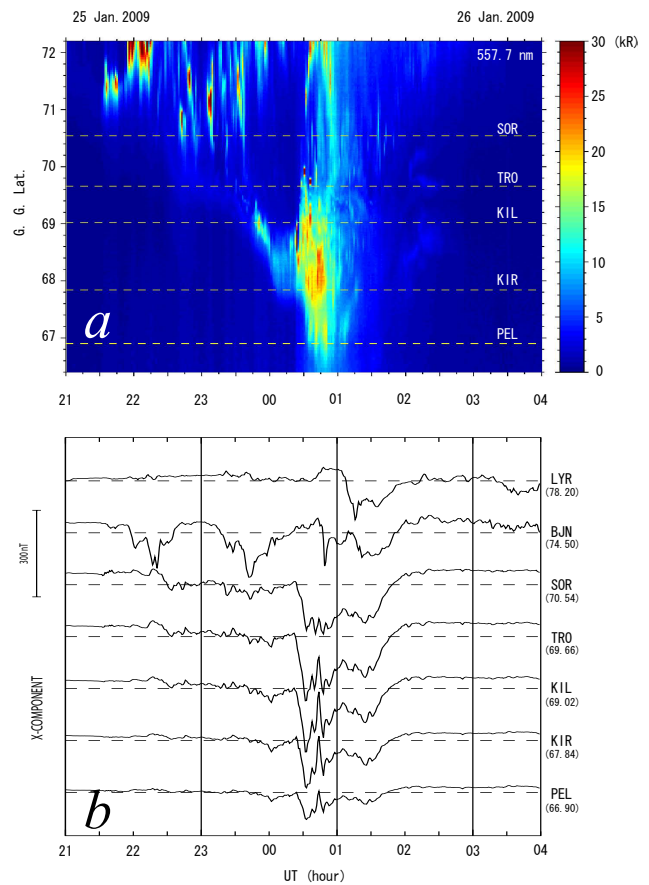


**Fig. 1.** (a) Keogram showing meridional auroral motion from the ASC ( $\lambda = 557.7$  nm) at the Tromsø EISCAT radar site from 21:00 UT on 25 January to 04:00 UT on 26 January 2009. The color scale corresponds to intensity (from 0 to 30 kR) as shown in the color bar. Horizontal dashed lines indicate the five magnetometer sites selected in panel (b). (b) Temporal variations in the x-component (N-S) of the geomagnetic field measured at seven sites of the IMAGE magnetometer chain from 21:00 UT on 25 January to 04:00 UT on 26 January 2009 in Longyearbyen (LYR), Bear Island (BJN), Sørøya (SOR), Tromsø (TRO), Kilpisjärvi (KIL), Kiruna (KIR), and Pello (PEL). The number in the bracket is geographic latitude for each site. The scale is illustrated at the left-hand-side.

to extend along the zonal direction. The pulsation sequence consisted of pulses with “on” time being shorter than “off” time, which is one of the typical characteristics of Type 1 or positive pulsations according to the classification proposed by Yamamoto and Oguti (1982).

The pulsating aurora for this event had 2–4 Hz modulations in intensity superimposed on the slower variations in the range of 50–200 mHz. This frequency combination has also been found in previous studies (Røyrvik, 1978; Sandahl et al., 1980; Yamamoto, 1988; Nemzek et al., 1995). The pulsating auroras did not have notable deformations; but sometimes showed so-called streaming. After 01:40 UT, the auroral luminosity faded away except for the northern edge of the all-sky image.

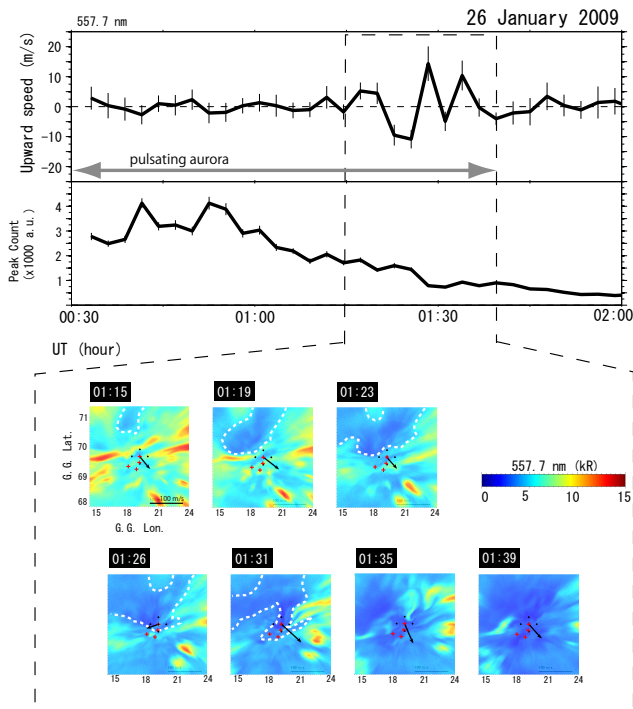


**Fig. 2.** Top and middle panels show the temporal variations in the vertical wind speed and the fringe peak count at the zenith, respectively, measured with the FPI (557.7 nm) from 00:30 to 02:00 UT on 26 January 2009. Vertical bars at each data point represent the  $2\sigma$  uncertainty (see in the text). The bottom color panels show the horizontal aurora images taken with the ASC at 557.7 nm from 01:15 to 01:39 UT during pulsating aurora (corresponding time interval is marked by black dashed line in the top two panels). The color scale of optical intensity is shown at the right middle. These images are mapped in geographic coordinate assuming the peak emission height is 110 km. The five black dots and the four red crosses indicate the location of the FPI and the EISCAT UHF radar observation positions, respectively. The black arrows correspond to the horizontal component of the FPI-derived neutral wind velocity (the scale is presented at the right bottom corner of the first panel from the left). White dashed lines in the colored panels are drawn to easily identify the darker area.

The top panel in Fig. 2 shows temporal variations in the vertical-wind speed measured with the FPI ( $\lambda = 557.7$  nm) from 00:30 to 02:00 UT. The vertical bar at each data point represents the  $2\sigma$  uncertainty, where  $\sigma$  is the standard deviation derived from 10 fringe values (see Sect. 2). To derive the vertical wind values, the running-average method was employed to the mean values calculated from the 10 fringe values. This is because variations in the room temperature of the FPI hut shift the FPI etalon gap, causing counterfeited temporal variations in the wind value typically longer than a few hours. To remove the longer trends, we used a running-average window length about 1-h time interval (22 data points). The middle panel shows temporal variations in the fringe peak count, which corresponds to the emission in-

tensity at the zenith measured with the FPI. The color panels present aurora images taken with the ASC ( $\lambda = 557.7$  nm) from 01:15 to 01:39 UT. They are mapped in geographic coordinates assuming an emission height of 110 km. The five black dots and four red crosses illustrate observation positions with the FPI and the EISCAT UHF radar, respectively, at 110 km height. Black arrows present the horizontal wind vector derived with the FPI.

Of particular interest is the fluctuation in the wind velocity that appears in a darker area within the pulsating aurora. While the auroral intensity gradually decreases with time at the zenith after 01:00 UT (as shown in the middle panel of Fig. 2), a darker area (enclosed by white dashed line in the colored panels of Fig. 2) develops and extends to the FPI observation area from the northwest side at 01:15 UT (the first colored-panel from the left). The darker area arrives at the zenith of the FPI at 01:26 UT (the fourth colored-panel) as the middle panel shows a small but clear drop of the fringe peak count at that time. As the darker area approaches to the zenith, the vertical speed clearly shows oscillations with amplitudes larger than  $10 \text{ m s}^{-1}$ . The vertical speed does not show notable oscillations for other time intervals shown here.

The horizontal neutral wind velocity also shows an obvious variation coinciding with the vertical speed fluctuation. Six of the seven wind vectors in Fig. 2 are directed southeastward. While all temporal variations in the horizontal component are not shown here, this southeastward wind lasted from 23:30 UT on 25 January to 02:30 UT on 26 January. However, the horizontal wind velocity at 01:26 UT (the fourth colored-panel) flows almost westward, completely different from the other wind vectors, then the wind velocity at 01:31 UT goes back to the southeastward direction but with a larger amplitude. These temporal variations appear approximately at the same time as the vertical-speed fluctuations.

One may think that the peak emission height in the darker area is from a higher altitude than that in the brighter area because the 557.7 nm emission can spread above 150 km. However, the emission rate above 150 km is lower than that in the E-region by about two orders of magnitude (Rees, 1984). The emission intensity measured with the ASC (557.7 nm) in the darker area is about 5 kR, which is unlikely for the emission at heights above 150 km.

A careful analysis is necessary for the horizontal component of the lower-thermospheric wind velocity because of the vertical shear of the horizontal wind velocity at E-region heights (e.g. Johnson and Virdi, 1991; Salah et al., 1991; Salah, 1994; Azeem and Johnson, 1997; Larsen, 2002; Fujiwara et al., 2004) and variations in the peak emission height of 557.7 nm. The vertical component is not affected significantly by the peak emission height change within the E-region because the vertical component does not have large vertical shear on average (Oyama et al., 2005). The FPI-derived vertical wind fluctuation is thus considered as one of the lower-thermospheric responses to the energy input and/or the momentum transfer into the lower thermosphere.

This result suggests that the lower thermospheric wind can quickly deviate from its large-scale motions in a localized area when the energy input and/or the momentum transfer occurred, even though on average the large-scale motion is predominant in the lower thermosphere.

### 3.2 Event 2: 19 January 2009

This section presents an event that shows lower-thermospheric wind fluctuations during pulsating aurora that appeared from 01:40 to 03:00 UT on 19 January 2009. Figure 3a is a keogram of ASC ( $\lambda = 557.7$  nm) images from 23:00 UT on 18 January to 06:00 UT on 19 January 2009. From 23:30 to 01:15 UT, a faint arc appeared along the northern horizon (around  $70.5^\circ$  N latitude) on the all-sky image measured in Tromsø and gradually moved toward the zenith increasing in luminosity. At about 01:25 UT, a bright “blob” appeared on the westward edge of an arc then propagating eastward along the arc. That blob might be a part of the initial brightening of the substorm breakup that occurred far westward from Tromsø. In about 15 min ( $\sim 01:40$  UT), most of the area seen in the all-sky camera, except for its southern and northern edges, was covered by spatio-temporally complex pulsating aurora. The pulsating aurora was observed until about 03:00 UT weakening in luminosity with time. Patchy faint tropospheric clouds passed over the zenith from 02:34 to 02:49 UT. However, pulsating aurora was visually identified in the all-sky TV camera data through the thin clouds.

The pulsating aurora moved mostly westward keeping its shape but streaming pulsation was not identified for this case. The predominant pulsating frequency was 0.5–1 Hz in this case. This temporal evolution of the auroral morphology is consistent with the x-component of the magnetometer data shown in Fig. 3b. The negative deviation (corresponding to the westward ionospheric current) coincides with enhancements of auroral intensity after 01:25 UT. Pulsating aurora appeared during the recovery phase of substorm.

For the event of 26 January 2009, fluctuations in the lower thermospheric wind velocity were found in a darker area associated with pulsating aurora. A similar signature as the 26 January case was also observed in the 19 January case. Figure 4 shows the vertical wind speed and the fringe peak count from 02:30 to 04:00 UT. Data observed during the cloudy period are shown in gray. The mapped aurora images are presented from 02:50 to 03:05 UT (corresponding to the time interval marked by black dashed line). Pulsating auroras have appeared approximately from 01:40 to 03:00 UT. During the appearance of pulsating auroras, the vertical wind speed does not have notable fluctuations except for the period from 02:50 to 03:00 UT. A decrease in the fringe peak count, or the auroral intensity, at 02:50 UT corresponds to the appearance of a darker area at the zenith as shown in the color panels. Upward wind speed greater than  $25 \text{ m s}^{-1}$  is seen at 02:54 UT. At that time, the darker area is at the zenith,

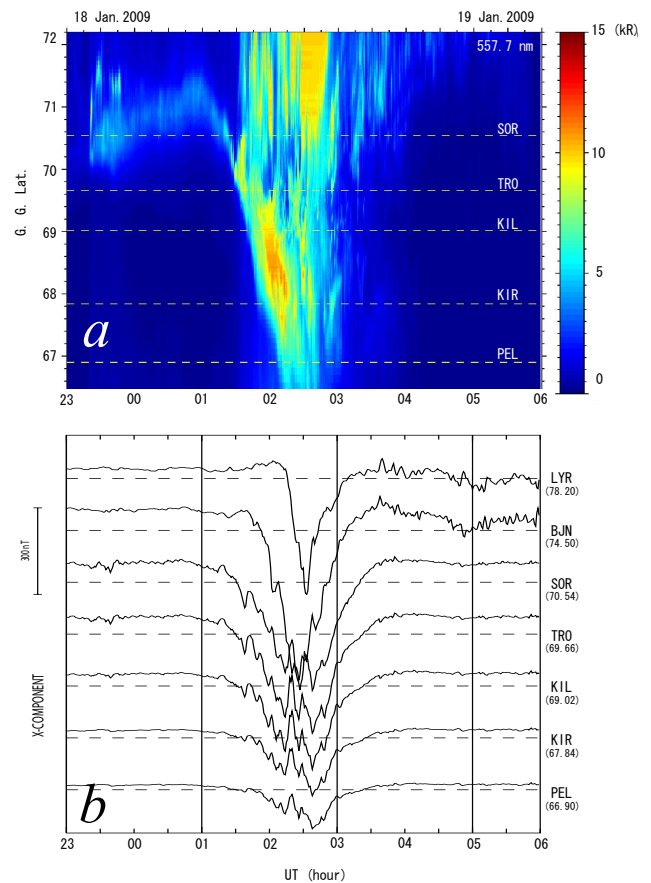


**Fig. 3.** Same as Fig. 1 but for time interval from 23:00 UT on 18 January to 06:00 UT on 19 January 2009. Note that the maximum of the color scale is 15 kR instead of 30 kR used in Fig. 1a.

which is almost surrounded by brighter patches except in the southwest side (see image at 02:53 UT). After 02:53 UT the vertical wind speed does not show notable fluctuations as the boundary between the darker and the brighter area gradually becomes unclear due to the decrease in auroral intensity.

The horizontal wind (illustrated by black arrows in the colored-panels of Fig. 4) flows southeastward from 02:50 to 03:05 UT. The southeastward wind has been predominant from 00:30 to 04:00 UT on 19 January though containing some fluctuations in the amplitude and the direction. The horizontal wind magnitude promptly responds to the appearance of the darker area in pulsating aurora in the event 2. The horizontal wind velocity seems to be fully accelerated by  $30 \text{ m s}^{-1}$  to the southeastward direction when the vertical wind speed reaches  $25 \text{ m s}^{-1}$ .

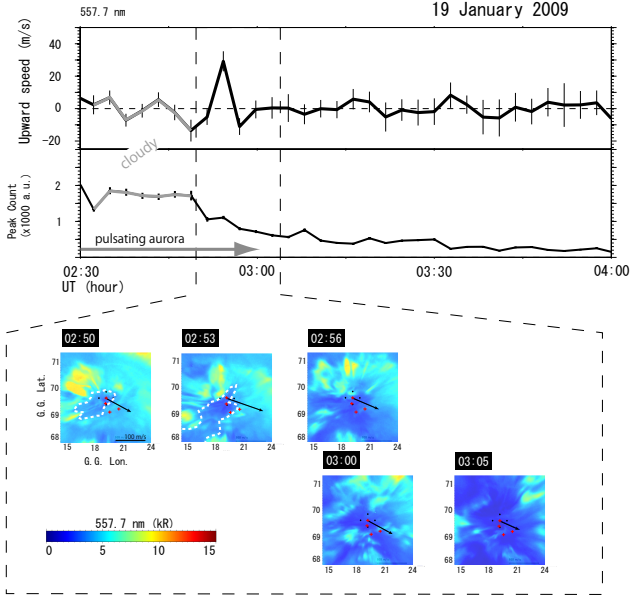


**Fig. 4.** Same as Fig. 2 but for the event on 19 January 2009. The vertical speed and the fringe peak count are made of data obtained from 02:30 to 04:00 UT. Data during the cloudy condition are plotted by gray curves in the top two panels. The mapped auroral images in the bottom color panels are made of data from 02:50 to 03:05 UT.

## 4 Discussion

### 4.1 Theory

This section discusses effects of the electric-field perturbation on ionospheric/thermospheric heating. Enhancement of the Joule heating rate by the electric-field perturbation and appearance of the electric-field perturbation during pulsating aurora have already been addressed by other researchers as mentioned in Sect. 1. The Joule heating process increases the thermospheric temperature even at the lower thermospheric heights (Shinagawa and Oyama, 2006), and the temperature increase can directly affect the wind dynamics due to modification of the pressure gradient (Oyama et al., 2008; Tsuda et al., 2009). Therefore we investigate the temperature variations induced by the electric-field perturbations.

We start from the ion momentum equation including the time derivative term as shown in Eq. (1).

$$m_i N_i \frac{d\mathbf{V}}{dt} = -\nabla P_i + m_i N_i \mathbf{g} + e N_i (\mathbf{E} + \mathbf{V} \times \mathbf{B}) - m_i N_i \nu_{in} (\mathbf{V} - \mathbf{U}) \quad (1)$$

where  $m_i$ ,  $N_i$ , and  $P_i$  are the mean ion mass, the ion density, and the ion pressure, respectively,  $e$  is the charge of electron,  $\nu_{in}$  is the ion-neutral collision frequency,  $\mathbf{V}$ ,  $\mathbf{g}$ ,  $\mathbf{E}$ ,  $\mathbf{B}$ , and  $\mathbf{U}$  are vectors of the ion velocity, the gravitational acceleration, the electric field, the magnetic field, and the neutral wind velocity, respectively. Substituting the relative speed of  $\mathbf{V} - \mathbf{U}$  by  $\mathbf{V}'$  and neglecting the diffusion velocity term, which is

the sum of the first and second terms of the right-hand-side in Eq. (1), provides the following equation:

$$\frac{d\mathbf{V}}{dt} = \frac{Be}{m_i} \left( \frac{\mathbf{E}'}{B} + \mathbf{V}' \times \mathbf{b} \right) - \nu_{in} \mathbf{V}' \quad (2)$$

where  $\mathbf{b}$  is the unit vector of  $\mathbf{B}$ , and  $\mathbf{E}'$  is equal to  $\mathbf{E} + \mathbf{U} \times \mathbf{B}$ . Since the ion energy equation, which is widely used to discuss the ionospheric/thermospheric heating process, includes a term related to square of  $\mathbf{V}'$ , the square of  $\mathbf{V}'$  is derived from Eq. (2). Equation (2) can be replaced by

$$\nu_{in} \mathbf{V}' - \Omega_i (\mathbf{V}' \times \mathbf{b}) = \Omega_i \left( \frac{\mathbf{E}'}{B} \right) - \frac{d\mathbf{V}}{dt} \quad (3)$$

$$\mathbf{V}' - k_i (\mathbf{V}' \times \mathbf{b}) = k_i \left( \frac{\mathbf{E}'}{B} \right) - \frac{1}{\nu_{in}} \frac{d\mathbf{V}}{dt} \quad (4)$$

then

$$(\mathbf{V}')^2 + k_i^2 \left\{ (\mathbf{V}')^2 - (\mathbf{V}'_{//})^2 \right\} = \left\{ \left( \frac{k_i}{B} \right) \mathbf{E}' - \left( \frac{1}{\nu_{in}} \frac{d\mathbf{V}}{dt} \right) \right\}^2 \quad (5)$$

where  $k_i$  is the ion mobility coefficient defined by  $\Omega_i/\nu_{in}$  ( $\Omega_i$  is the ion gyrofrequency). Since the field-aligned ion motion does not play an important role for the frictional heating process compared with the perpendicular component (almost equivalent to the horizontal component), we can ignore the last term of the left-hand-side of Eq. (5). Then Eq. (5) can be written as Eq. (6):

$$(\mathbf{V}')^2 = \frac{1}{1+k_i^2} \left\{ \left( \frac{k_i}{B} \right) \mathbf{E}' - \left( \frac{1}{\nu_{in}} \frac{d\mathbf{V}}{dt} \right) \right\}^2 \quad (6)$$

The time derivative term in Eq. (6) may be expressed as Eq. (7) if  $\mathbf{B}$  is stable.

$$\frac{d\mathbf{V}}{dt} = \frac{1}{B^2} \left( \frac{d\mathbf{E}}{dt} \times \mathbf{B} \right) \quad (7)$$

Equation (6) can be modified by substituting Eq. (7):

$$(\mathbf{V}')^2 = \frac{1}{1+k_i^2} \left\{ \left( \frac{k_i}{B} \right) \mathbf{E}' - \left( \frac{1}{\nu_{in} B^2} \frac{d\mathbf{E}}{dt} \times \mathbf{B} \right) \right\}^2 \quad (8)$$

then

$$(\mathbf{V}')^2 = \frac{1}{1+k_i^2} \left[ \left( \frac{k_i}{B} \right)^2 (\mathbf{E}')^2 - \frac{2k_i}{\nu_{in} B^3} \left( \frac{d\mathbf{E}}{dt} \cdot (\mathbf{B} \times \mathbf{E}') \right) + \frac{1}{\nu_{in}^2 B^4} \left\{ \left( \frac{d\mathbf{E}}{dt} \right)^2 B^2 - \left( \mathbf{B} \cdot \frac{d\mathbf{E}}{dt} \right)^2 \right\} \right] \quad (9)$$

For simplicity, we assume that magnitude of the electric field varies with time but not for the direction. In this case the time derivative term of the electric field in Eq. (9) can be given using the unit vector of  $\mathbf{e}$  by

$$\frac{d\mathbf{E}}{dt} = \frac{dE}{dt} \mathbf{e} \quad (10)$$

Then Eq. (9) can be replaced as following:

$$(\mathbf{V}')^2 = \frac{1}{1+k_i^2} \left\{ \left( \frac{k_i}{B} \right)^2 (\mathbf{E}')^2 - \frac{2k_i}{v_{in}B^3} \left( \frac{dE}{dt} \mathbf{e} \cdot (\mathbf{B} \times \mathbf{E}') \right) + \left( \frac{1}{v_{in}B} \frac{dE}{dt} \right)^2 \right\}, \quad (11)$$

then

$$(\mathbf{V}')^2 = \frac{1}{1+k_i^2} \left\{ \left( \frac{k_i}{B} \right)^2 (\mathbf{E}')^2 - \frac{2k_i}{v_{in}B} \frac{dE}{dt} U_E + \left( \frac{1}{v_{in}B} \frac{dE}{dt} \right)^2 \right\} \quad (12)$$

where  $U_E$  is the neutral wind parallel to the electric field. The second term between the braces on the right-hand-side of Eq. (12) is considerably smaller than the third one by 5–6 orders of magnitude. The ion energy equation provides the ion temperature variation, which is a function of the relative velocity  $\mathbf{V}'$  (St.-Maurice and Hanson, 1982; Oyama et al., 2004, 2009). Since Eq. (12) shows that the relative velocity is a function of the time derivative of the electric field, which corresponds to the electric-field perturbation, the ion-temperature variation can be finally expressed as Eq. (13):

$$T_{\text{fric-dt}} = \frac{m_n}{3k_B} \frac{1}{1+k_i^2} \left( \frac{1}{v_{in}B} \frac{dE}{dt} \right)^2. \quad (13)$$

Figure 5 shows the ion-temperature increase estimated from Eq. (13) as a function of the electric field perturbation amplitude and frequency. While there is no experimental evidence regarding amplitude of the electric-field oscillation for the two events, a magnetospheric observation with FAST satellite shows that the amplitude at 10 Hz is about  $30 \text{ mV m}^{-1}$  increasing with decreasing in the oscillation frequency (Nakajima et al., 2008). In this case the ion temperature may increase by 20–30 K according to Fig. 5. We compared with the ion temperature measured with the EISCAT radar, but clear increases were not identified for the time interval of the vertical-wind fluctuations. This may be because the measurement uncertainty of the EISCAT ion temperature at that time is almost equivalent to 20–30 K. We should note that a neutral temperature increase by a few degrees is enough to change the wind dynamics in the lower thermosphere (Sun et al., 1995; Shinagawa and Oyama, 2006). However, we are not sure if the increased thermal energy of ions is enough to elevate that of neutral particles or the neutral temperature. More theoretical work is needed to understand the energy transfer process between ions and neutral particles.

#### 4.2 Generation mechanism of the lower-thermospheric wind fluctuations

The two events clearly demonstrate that notable fluctuations in the lower thermospheric wind velocity are measured in association with pulsating aurora. To the best of our knowledge, there is no literature regarding lower-thermospheric

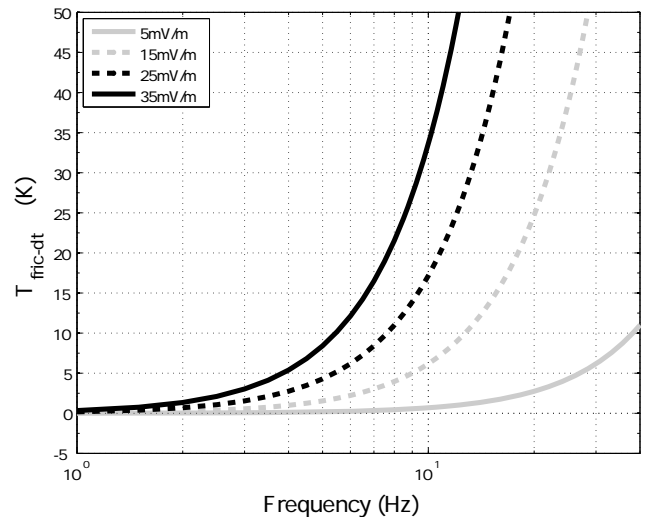


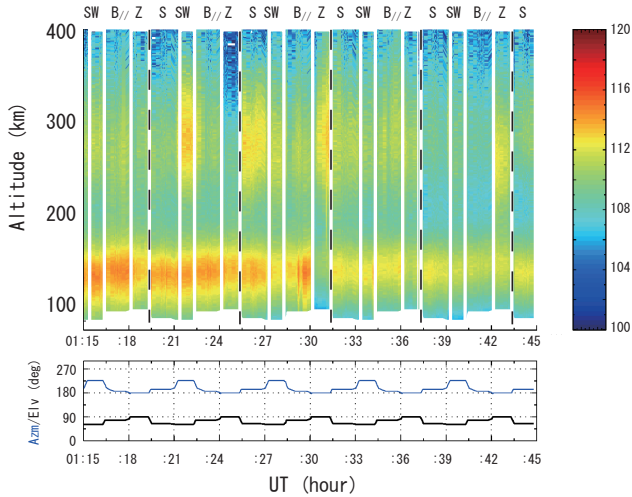
**Fig. 5.** Profile of the ion-temperature increase estimated with Eq. (13) taking into account the time derivative term of the electric field. The oscillation amplitude is classified by gray-scale color and line style.

wind fluctuations during pulsating aurora. Both events have occurred in the depression phase of the auroral activity or the recovery phase of substorms. Since this paper shows only two events, we need more experimental evidence to assess statistically the validity of these observations. However, it is useful to consider possible mechanisms that may explain these data. We suggest that previous hypotheses considering Joule energy dissipation to explain wind fluctuations may not be appropriate in this case because the electric fields measured with the EISCAT UHF radar for the two events are relatively small (at most  $20 \text{ mV m}^{-1}$ ; not shown here). However, the Joule heating rate can be increased by electric field perturbations as suggested by Fig. 5.

The EISCAT radar data present signatures that suggest the presence of electric-field perturbations. Figure 6 shows the backscatter power (colored panels) for 30 min (from 01:15 to 01:45 UT for event 1 and from 02:45 to 03:15 UT in the event 2). The antenna configuration is shown in the bottom panel for azimuth (blue) and elevation (black) angles. For convenience, vertical dotted lines mark each antenna sequence, and antenna directions are illustrated by symbols at the top of the colored panel.

Clear enhancements in the backscatter echo power can be seen in the E-region because of high energy particle precipitation causing the pulsating aurora. The gradual decrease in the E-region backscatter echo power is consistent with attenuation of the fringe peak count shown in Figs. 2 and 4. Of particular interest is the F-region backscatter echo power, which sporadically increases independently from the E-region variations. Enhancements of the F-region backscatter echo power do not always appear at a specific antenna position. Observation with antenna at zenith at 01:31 UT

26 January 2009



19 January 2009

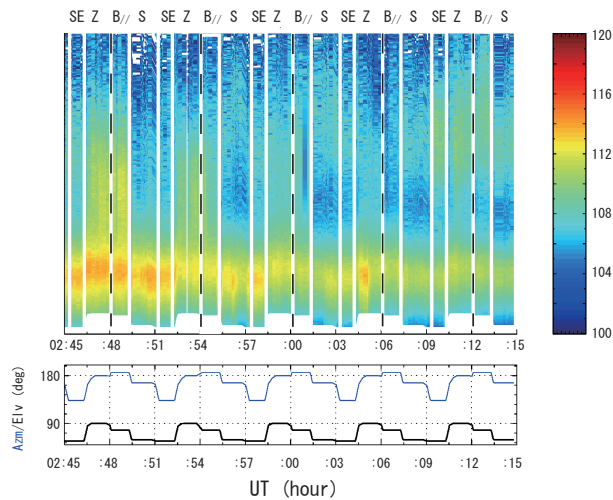
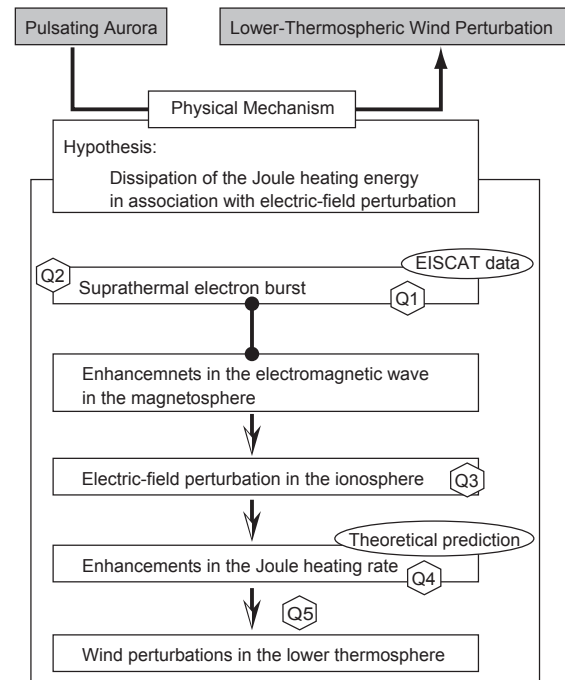


**Fig. 6.** Backscatter echo power in dB measured with the EISCAT UHF radar from 01:15 to 01:45 UT on 26 January 2009 (upper color panel) and from 02:45 to 03:15 UT on 19 January 2009 (lower color panel). The antenna beam direction is marked by individual symbols at the top of the color panel (See in Table 1 for symbols' description). The vertical white lines show the boundary from a beam direction to the next one. The temporal variations in the azimuth and elevation angles are plotted in the bottom panels. The vertical dotted lines indicate each antenna sequence.

on 26 January presents a sudden depression in the E-region backscatter echo power but increase in the F-region one. Around that time, the FPI-derived wind velocity has notable fluctuations as shown in Fig. 2. The backscatter echo power also presents such a synchronized variations between E- and F-regions at 02:53 UT on 19 January when the FPI measured large upward speed as shown in Fig. 4.



- Q1 What is the ionospheric response to the suprathermal electron burst?
- Q2 Can the suprathermal electron burst coexist with pulsating aurora?
- Q3 Can the electromagnetic wave in the magnetosphere penetrate into the ionosphere?
- Q4 Can we find observation evidences to prove increases in the ionospheric/thermospheric thermal energy?
- Q5 Is the thermal energy enough to modify winds in the lower thermosphere?

**Fig. 7.** Summary of the hypothesis in this paper. Experimental evidences of the pulsating aurora and the lower-thermospheric wind perturbation are hatched by gray. The physical mechanism proposed here has four steps from the suprathermal electron burst, which was predicted by the EISCAT radar data, to the wind perturbation measured with the FPI. Five open questions to be studied in more detail are enumerated.

The precipitation particle energy required to cause F-region enhancements must be lower than 1 keV according to the stopping-height theory (Rees, 1989). This is important experimental information because sporadic precipitation of electrons of energy less than 1 keV may be related to the suprathermal electron bursts (Johnstone and Winningham, 1982). The suprathermal electron burst coincides with the electric- and magnetic-field perturbations or Alfvén waves in the magnetosphere (Dombeck et al., 2005). Simultaneous observations with FAST and Polar satellites (Nakajima et al., 2008) suggest that the Alfvén waves at oscillation frequency higher than 1 Hz seem to be generated between FAST (about 3500 km) and Polar (about 7 Re) altitudes. The amplitude of the electric-field perturbation is dependent on events; but some examples of the FAST observation present the amplitude of  $30 \text{ mV m}^{-1}$  at 10 Hz for the electric-field perturbation.

While the observation showed coexistence of the lower-thermospheric wind perturbation with pulsating aurora, the hypothesis connecting these two phenomena is based on several assumptions. Figure 7 summarizes the observation results and discussion in this paper. The hypothesis is that the energy that causes perturbations in the lower-thermospheric wind velocity during pulsating aurora is dissipated by Joule heating in association with electric-field perturbation. The EISCAT radar presents sporadic enhancements in the F-region density (see Fig. 6), which are regarded as an ionospheric response to the suprathermal electron burst. Satellite observations in the magnetosphere suggest that the suprathermal electron burst coincides with enhancements in the electromagnetic wave or electric/magnetic field perturbations (Dombeck et al., 2005). Theoretical equations predict enhancements in the ion temperature due to electric-field perturbations at lower-thermospheric heights. The thermal energy of ions is transferred to neutral particles, causing perturbations in the lower thermospheric wind velocity.

The hypothesis suggests future directions to be investigated in more detail. They are marked by Q1 to Q5 in Fig. 7. Q1 and Q2 are “What is the ionospheric response to the suprathermal electron burst?” and “Can the suprathermal electron burst coexist with pulsating aurora?” This paper analyzed the backscatter echo power measured with the EISCAT radar in order to find ionospheric signatures during pulsating aurora. While magnetospheric signatures of the suprathermal electron burst have been reported in many publications, there are no publication regarding the ionospheric response. Furthermore there is no experimental evidence that shows a relationship between pulsating aurora and the suprathermal electron burst. Q3 is “Can the electromagnetic wave in the magnetosphere penetrate into the ionosphere?” It is well known that large-scale electric fields map down on the ionosphere (Lyons, 1980; Weimer et al., 1985). However, high-frequency components of the electric field (higher than  $\sim 10$  Hz) may be attenuated considerably before getting down to the ionosphere (Reid, 1965). Q4 is “Can we find observational evidences to prove increases in the ionospheric/thermospheric thermal energy?” The Joule/particle heating rate can be estimated using, for example, IS-radar data. However, it is difficult to understand the relationship between the heating rate and the temperature variation because the temperature elevation may be smaller than the measurement uncertainty of the IS radar at E-region heights. Q5 is “Is the thermal energy enough to modify winds in the lower thermosphere?” The theoretical equation in this paper suggests large temperature enhancements in excess of a few tens of degrees due to the electric-field perturbation. However, the prediction should be directly proved by observation data.

Direct heating due to particle precipitation, may also be significant but we think that it is of secondary importance as estimated below. Estimation of the particle heating rate has been established under several assumptions, including steady state conditions in the ionosphere, that is, neglecting

the time-derivative term in the continuity equation (Vickrey et al., 1982). However, more theoretical work needs to be done regarding the effects of electron-density oscillation on the particle heating rate. While this paper does not address this issue, it should be studied in future. As reference, the height-integrated particle heating rate derived from EISCAT radar data for the two events is at most  $3 \text{ mW m}^{-2}$ , which is only  $\sim 10\%$  of the typical Joule heating rate for active periods (Oyama et al., 2008; Kurihara et al., 2009).

To prove the hypothesis it is necessary to have simultaneous observation between the ionosphere and the magnetosphere during pulsating aurora. While the backscatter echo power measured with the EISCAT radar is analyzed in this paper to find evidence of the suprathermal electron bursts, there are some publications that propose other mechanisms as the cause of F-region enhancements during pulsating aurora. Prasad et al. (1983) and Evans et al. (1987) suggest that the low-energy ( $< 1 \text{ keV}$ ) particle precipitation during pulsating aurora is caused by secondary electrons produced in the conjugate hemisphere. Williams et al. (2006) propose another mechanism, which suggests that secondary electrons produced in the lower ionosphere travel upward along the magnetic field line then reflecting backward or downward at the upper ionosphere boundary due to a parallel electric field. On the other hand, Lu et al. (1991) report observations of the suprathermal electron bursts in the diffuse aurora, which typically contains pulsating aurora. Sato et al. (2002) have observed inverted-V structure over pulsating aurora with peaks downward energy in the range of  $0.1\text{--}1 \text{ keV}$ , which can cause ionization in the F-region. There are at least four hypotheses available to explain the low-energy particle precipitation during pulsating aurora.

## 5 Summary and conclusions

We conducted simultaneous observations using an FPI, an ASC, and the EISCAT radar in Tromsø, Norway during the DELTA-2 campaign in January 2009. This paper concentrated on two events during periods of pulsating aurora. The FPI ( $\lambda = 557.7 \text{ nm}$ ) observed notable fluctuations of the lower-thermospheric wind velocity in a darker area that appeared within pulsating aurora. At that time, the vertical wind speed clearly showed oscillations with amplitudes larger than  $10 \text{ m s}^{-1}$ . The electric field magnitude measured with the EISCAT radar for the two events was at most  $20 \text{ mV m}^{-1}$ . This value is considerably smaller than the electric field adopted in previous simulation studies for calculating the Joule heating rate. This paper discussed effects of the inferred electric-field perturbations because the F-region backscatter echo power measured with the EISCAT UHF radar suggested the presence of suprathermal electron burst. This magnetospheric phenomenon tends to coincide with increases in amplitude of the electromagnetic wave on the order of  $10 \text{ Hz}$  or higher. The theoretical prediction suggested

that the ion-temperature increased by more than 20–30 K with the Joule heating process created by fluctuating electric field at a frequency of about 10 Hz or higher. However, the data set available for the conclusion is rather limited, so more experimental data should be collected to assess the validity of the hypothesis proposed in this paper.

*Acknowledgements.* We are indebted to the director and staff of EISCAT for operating the facility and supplying the data. EISCAT is an International Association supported by China (CRIRP), Finland (SA), the Federal Republic of Germany (DFG), Japan (STEL and NIPR), Norway (NFR), Sweden (VR) and the United Kingdom (PPARC). We thank the institutes who maintain the IMAGE magnetometer array. We are pleased to acknowledge the assistance of A. Nakajima regarding the suprathermal electron bursts measured with satellites. We thank T. Katoh, M. Satoh, Y. Katoh, H. Hamaguchi, and Y. Yamamoto, of STEL, Nagoya University, for their skillful supports on development of the ASC and the FPI. The high-speed ATV is operated by National Institute of Polar Research, Japan. This research has been supported by a Grant-in-Aid for Scientific Research (17340145, 18403010, 18403011, 20244080, and 22403010) and Special Funds for Education and Research (Energy Transport Processes in Geospace) from MEXT, Japan. This research was partially supported by the Grant-in-Aid for Nagoya University Global COE Program, “Quest for Fundamental Principles in the Universe: from Particles to the Solar System and the Cosmos”, from MEXT, Japan.

Topical Editor K. Kauristie thanks A. Brekke and another anonymous referee for their help in evaluating this paper.

## References

- Azeem, S. M. I. and Johnson, R. M.: Lower thermospheric neutral winds at Sondre Stromfjord: A seasonal analysis, *J. Geophys. Res.*, 102, 7379–7397, 1997.
- Brekke, A. and Kamide, Y.: On the relationship between Joule and frictional heating in the polar ionosphere, *J. Atmos. Terr. Phys.*, 58(1–4), 139–143, 1996.
- Brekke, A.: *Physics of the upper polar atmosphere*, Wiley-Praxis, 1997.
- Codrescu, M. V., Fuller-Rowell, T. J., and Foster, J. C.: On the importance of E-field variability for Joule heating in the high-latitude thermosphere, *Geophys. Res. Lett.*, 22(17), 2393–2396, 1995.
- Codrescu, M. V., Fuller-Rowell, T. J., Foster, J. C., Holt, J. M., and Cariglia, S. J.: Electric field variability associated with the Millstone Hill electric field model, *J. Geophys. Res.*, 105(A3), 5265–5273, 2000.
- Davidson, G. T.: Pitch-angle diffusion and the origin of temporal and spatial structures in morningside aurorae, *Space Sci. Rev.*, 53, 45–82, 1990.
- Dombeck, J., Cattell, C., Wygant, J. R., Keiling, A., and Scudder, J.: Alfvén waves and Poynting flux observed simultaneously by Polar and FAST in the plasma sheet boundary layer, *J. Geophys. Res.*, 110, A12S90, doi:10.1029/2005JA011269, 2005.
- Evans, D. S., Davidson, G. T., Voss, H. D., Imhof, W. L., Mobilia, J., and Chiu, Y. T.: Interpretation of electron spectra in morning side pulsating aurorae, *J. Geophys. Res.*, 92, 12295–12306, 1987.
- Fujiwara, H., Maeda, S., Suzuki, M., Nozawa, S., and Fukunishi, H.: Estimation of electromagnetic and turbulent energy dissipation rates under the existence of strong wind shears in the polar lower thermosphere from the European Incoherent Scatter (EISCAT) Svalbard radar observations, *J. Geophys. Res.*, 109, A07306, doi:10.1029/2003JA010046, 2004.
- Hosokawa, K., Kadokura, A., Sato, N., Milan, S. E., Lester, M., Bjornsson, G., and Saemundsson, Th.: Electric field modulation behind pulsating aurora, *J. Geophys. Res.*, 113, A11322, doi:10.1029/2008JA013601, 2008.
- Hosokawa, K., Ogawa, Y., Kadokura, A., Miyaoka, H., and Sato, N.: Modulation of ionospheric conductance and electric field associated with pulsating aurora, *J. Geophys. Res.*, 115, A03201, doi:10.1029/2009JA014683, 2010.
- Ishii, M., Kubota, M., Conde, M., Smith, R. W., and Krynicki, M.: Vertical wind distribution in the polar thermosphere during Horizontal E Region Experiment (HEX) campaign, *J. Geophys. Res.*, 109, A12311, doi:10.1029/2004JA010657, 2004.
- Johnson, R. M. and Virdi, T. S.: High-latitude lower thermospheric neutral winds at EISCAT and Sondrestrom during LTCS, *J. Geophys. Res.*, 96, 1099–1116, 1991.
- Johnstone, A. D. and Winningham, J. D.: Satellite observations of suprathermal electron bursts, *J. Geophys. Res.*, 87(A4), 2321–2329, 1982.
- Kosch, M. J., Anderson, C., Makarevich, R. A., Carter, B. A., Fiori, R. A. D., Conde, M., Dyson, P. L., and Davies, T.: First E-region observations of meso-scale neutral wind interaction with auroral arcs, *J. Geophys. Res.*, 115, A2, doi:10.1029/2009JA014697, 2010.
- Kurihara, J., Oyama, S., Nozawa, S., Tsuda, T. T., Fujii, R., Ogawa, Y., Miyaoka, H., Iwagami, N., Abe, T., Oyama, K.-I., Kosch, M., Aruliah, A., Griffin, E., and Kauristie, K.: Temperature enhancements and vertical winds in the lower thermosphere associated with auroral heating during the Dynamics and Energetics of the Lower Thermosphere in Aurora (DELTA) campaign, *J. Geophys. Res.*, 114, A12306, doi:10.1029/2009JA014392, 2009.
- Larsen, M. F.: Winds and shears in the mesosphere and lower thermosphere: Results from four decades of chemical release wind measurements, *J. Geophys. Res.*, 107(A8), 1215, doi:10.1029/2001JA000218, 2002.
- Lu, G., Reiff, P. H., Burch, J. L., and Winningham, D.: On the auroral current-voltage relationship, *J. Geophys. Res.*, 96(A3), 3523–3531, 1991.
- Matsuo, T., Richmond, A. D., and Nychka, D. W.: Modes of high-latitude electric field variability derived from DE-2 measurements: Empirical Orthogonal Function (EOF) analysis, *Geophys. Res. Lett.*, 29(7), 1107, doi:10.1029/2001GL014077, 2002.
- Lyons, L. R.: Generation of large-scale regions of auroral currents, electric potentials, and precipitation by the divergence of the convection electric field, *J. Geophys. Res.*, 85(A1), 17–24, 1980.
- Matsuo, T., Richmond, A. D., and Hensel, K.: High-latitude ionospheric electric field variability and electric potential derived from DE-2 plasma drift measurements: Dependence on IMF and dipole tilt, *J. Geophys. Res.*, 108(A1), 1005, doi:10.1029/2002JA009429, 2003.
- Matsuo, T., Richmond, A. D., and Lu, G.: Optimal interpolation analysis of high-latitude ionospheric electrodynamics using empirical orthogonal functions: Estimation of dominant modes of

- variability and temporal scales of large-scale electric fields, *J. Geophys. Res.*, 110, A06301, doi:10.1029/2004JA010531, 2005.
- Matsuo, T. and Richmond, A. D.: Effects of high-latitude ionospheric electric field variability on global thermospheric Joule heating and mechanical energy transfer rate, *J. Geophys. Res.*, 113, A07309, doi:10.1029/2007JA012993, 2008.
- Nakajima, A., Shiokawa, K., Seki, K., McFadden, J. P., Carlson, C. W., Strangeway, R. J., and Yumoto, K.: Particle and field characteristics of broadband electrons observed by the FAST satellite during geomagnetic storms: A multievent study, *J. Geophys. Res.*, 113, A6, doi:10.1029/2007JA013001, 2008.
- Nemzek, R. J., Nakamura, R., Baker, D. N., Belian, R. D., McComas, D. J., Thomsen, M. F., and Yamamoto, T.: The relationship between pulsating auroras observed from the ground and energetic electrons and plasma density measured at geosynchronous orbit, *J. Geophys. Res.*, 100(A12), 23935–23944, 1995.
- Omholt, A.: *Physics and chemistry in space Volume 4, The Optical Aurora*, Springer, 1971.
- Oyama, S., Lathuillere, C., Maeda, S., and Watkins, B. J.: Summer-winter dependences of day-night differences in the ion temperature in the polar upper F region, *Geophys. Res. Lett.*, 31, L05806, doi:10.1029/2003GL018820, 2004.
- Oyama, S., Watkins, B. J., Nozawa, S., Maeda, S., and Conde, M.: Vertical ion motion observed with incoherent scatter radars in the polar lower ionosphere, *J. Geophys. Res.*, 110, A04302, doi:10.1029/2004JA010705, 2005.
- Oyama, S., Watkins, B. J., Maeda, S., Shinagawa, H., Nozawa, S., Ogawa, Y., Brekke, A., Lathuillere, C., and Kofman, W.: Generation of the lower-thermospheric vertical wind estimated with the EISCAT KST radar at high latitudes during periods of moderate geomagnetic disturbance, *Ann. Geophys.*, 26, 1491–1505, doi:10.5194/angeo-26-1491-2008, 2008.
- Oyama, S., Tsuda, T. T., Sakanoi, T., Obuchi, Y., Asamura, K., Hirahara, M., Yamazaki, A., Kasaba, Y., Fujii, R., Nozawa, S., and Watkins, B. J.: Spatial evolution of frictional heating and the predicted thermospheric-wind effects in the vicinity of an auroral arc measured with the Sondrestrom incoherent-scatter radar and the Reimei satellite, *J. Geophys. Res.*, 114, A07311, doi:10.1029/2009JA014091, 2009.
- Prasad, S. S., Strickland, D. J., and Chiu, Y. T.: Auroral electron interaction with the atmosphere in the presence of conjugate field-aligned electrostatic potentials, *J. Geophys. Res.*, 88, 4123–4130, 1983.
- Reid, G. C.: Ionospheric effects of electrostatic fields generated in the outer magnetosphere, *Radio Sci.*, 69D(6), 827–837, 1965.
- Rees, M. H.: Excitation of  $O(^1S)$  and emission of 5577 Å radiation in aurora, *Planet. Space Sci.*, 32(3), 373–378, 1984.
- Rees, M. H.: *Physics and chemistry of the upper atmosphere*, Cambridge University Press, 1989.
- Røyrvik, O.: Instabilities in pitch angle diffusion and their possible relation to a 3 Hz modulation in pulsating aurora, *J. Atmos. Terr. Phys.*, 40, 1309–1321, 1978.
- Salah, J. E.: Variability of winds and temperatures in the lower thermosphere, *J. Atmos. Terr. Phys.*, 56(10), 1327–1337, 1994.
- Salah, J. E., Johnson, R. M., and Tepley, C. A.: Coordinated incoherent scatter radar observations of the semidiurnal tide in the lower thermosphere, *J. Geophys. Res.*, 96, 1071–1080, 1991.
- Sandahl, I., Eliasson, L., and Jundin, R.: Rocket observations of precipitating electrons over a pulsating aurora, *Geophys. Res. Lett.*, 7(5), 309–312, 1980.
- Sangalli, L., Knudsen, D. J., Larsen, M. F., Zhan, T., Pfaff, R. F., and Rowland, D.: Rocket-based measurements of ion velocity, neutral wind, and electric field in the collisional transition region of the auroral ionosphere, *J. Geophys. Res.*, 114, A04306, doi:10.1029/2008JA013757, 2009.
- Sato, N., Wright, D. M., Ebihara, Y., Sato, M., Murata, Y., Doi, H., Saemundsson, T., Milan, S. E., Lester, M., and Carlson, C. W.: Direct comparison of pulsating aurora observed simultaneously by the FAST satellite and from the ground at Syowa, *Geophys. Res. Lett.*, 29, 2041, doi:10.1029/2002GL015615, 2002.
- Shepherd, S. G., Ruohoniemi, J. M., and Greenwald, R. A.: Direct measurements of the ionospheric convection variability near the cusp/throat, *Geophys. Res. Lett.*, 30(21), 2109, doi:10.1029/2003GL017668, 2003.
- Shinagawa, H. and Oyama, S.: A two-dimensional simulation of thermospheric vertical winds in the vicinity of an auroral arc, *Earth Planets Space*, 58, 1173–1181, 2006.
- Shiokawa, K., Kadota, T., Otsuka, Y., Ogawa, T., Nakamura, T., and Fukao, S.: A two-channel Fabry-Perot interferometer with thermoelectric-cooled CCD detectors for neutral wind measurement in the upper atmosphere, *Earth Planets Space*, 55, 271–275, 2003.
- Shiokawa, K., Otsuka, Y., and Ogawa, T.: Propagation characteristics of nighttime mesospheric and thermospheric waves observed by optical mesosphere thermosphere imagers at middle and low latitudes, *Earth Planets Space*, 61, 479–491, 2009.
- Stenbaek-Nielsen, H. C.: Pulsating aurora: The importance of the ionosphere, *Geophys. Res. Lett.*, 7(5), 353–356, 1980.
- St.-Maurice, J. P. and Hanson, W. B.: Ion frictional heating at high latitudes and its possible use for an in situ determination of neutral thermospheric winds and temperature, *J. Geophys. Res.*, 87, 7580–7602, 1982.
- Sun, Z. P., Turco, R. P., Walterscheid, R. L., Venkateswaran, S. V., and Jones, P. W.: Thermospheric response to morningside diffuse aurora: High-resolution three-dimensional simulations, *J. Geophys. Res.*, 100, 23779–23793, 1995.
- Tsuda, T. T., Nozawa, S., Oyama, S., Motoba, T., Ogawa, Y., Shinagawa, H., Nishitani, N., Hosokawa, K., Sato, N., Lester, M., and Fujii, R.: Acceleration mechanism of high-speed neutral wind observed in the polar lower thermosphere, *J. Geophys. Res.*, 114, A04322, doi:10.1029/2008JA013867, 2009.
- Vickrey, J. F., Vondrak, R. R., and Matthews, S. J.: Energy deposition by precipitating particles and Joule dissipation in the auroral ionosphere, *J. Geophys. Res.*, 87(A7), 5184–5196, 1982.
- Weimer, D. R., Goertz, C. K., Gurnett, D. A., Maynard, N. C., and Burch, J. L.: Auroral zone electric fields from DE 1 and 2 at magnetic conjunctions, *J. Geophys. Res.*, 90(A8), 7479–7494, 1985.
- Williams, J. D., MacDonald, E., McCarthy, M., Peticolas, L., and Parks, G. K.: Parallel electric fields inferred during a pulsating aurora, *Ann. Geophys.*, 24, 1829–1837, doi:10.5194/angeo-24-1829-2006, 2006.
- Yamamoto, T. and Oguti, T.: Recurrent fast motions of pulsating auroral patches 1. A case study on optical and quantitative characteristics during a slightly active period, *J. Geophys. Res.*, 87(A9), 7603–7614, 1982.
- Yamamoto, T.: On the temporal fluctuations of pulsating auroral luminosity, *J. Geophys. Res.*, 93(A2), 897–911, 1988.